



Braggs, Scherre, Williamson–Hall and SSP Analyses to Estimate the Variation of Crystallites Sizes and Lattice Constants for ZnO Nanoparticles Synthesized at different Temperatures

Nadia A. Abdulrahman^{1*}, Namir I. A. Haddad²

Abstract

This work presents crystallites characterization via XRD spectroscopy for ZnO nanoparticles previously prepared via hydrothermal technique at four different temperatures of 70, 100, 130 and 160 °C. As an industrial semiconductor, crystallite characterization is essential to rationally tune ZnO optical, mechanical, electrical and chemical properties. Braggs angles were used to estimate the internal distances, lattice constants and unit cell volumes. Scherrer equation was used to estimate crystallites sizes and the number of unit cells inside a single crystallite. Williamson Hall analysis was used to estimate crystallites strain, crystallites stress and crystallites energy density. And finally, SSP analysis was used to estimate the relation between crystallites sizes and crystallites strain. In general, XRD spectroscopy has indicated an average crystallite size of 40 nm with a short elongated hexagonal unit cell which agglomerated as wurtzite like shapes. SEM images have indicated a gradual growth for ZnO nanoparticles starting at > 40 to end up at > 500 nm as temperatures increased from 70 to 160 °C.

53

Key Words: ZnO Nanoparticles, ZnO Crystallites, Semiconductors, XRD Crystallography, Scherrer Equation, WH Analysis, SSP Analysis.

DOI Number: 10.14704/nq.2020.18.1.NQ20107

NeuroQuantology 2020; 18(1):53-63

Introduction

Zinc oxide, is an inorganic compound chemically symbolised as ZnO, it is a white powder known with several other non-scientific names such as Chinese white, philosopher's wool and Flowers of zinc [1,2]. Having as several as such non-scientific names indicates its wide use by industrial sectors. ZnO is a cheap compound and chemically stable with high melting point of 1975 °C. In comparison to conventional semiconductors, ZnO is considered as a semiconductor with wide band gap energy of 3.37 eV; which is why it is capable to be used at high temperatures, frequencies and voltages [3].

ZnO is a photoluminescence emitter with a large exciton binding energy of 60meV; which simply means intense photoluminescence emitting at room temperature or even higher [4, 5]. Interestingly, it is not that hard to have appreciable amounts and well-designed of ZnO particles with different sizes and different shapes at the range of nanometer length scale. On top, ZnO is a crystallite i.e. it could be studied precisely, and hence, its optical, mechanical, electrical and chemical properties could be rationally tuned.

Corresponding author: Nadia A. Abdulrahman

Address: ¹Department of Chemistry/ College of Science/ University of Baghdad/ Iraq; ²Department of Chemistry/ College of Science/ University of Baghdad/ Iraq.

¹E-mail: Nadiaabdulrahman73@yahoo.com

Relevant conflicts of interest/financial disclosures: The authors declare that the research was conducted in the absence of any commercial or financial relationships that could be construed as a potential conflict of interest.

Received: 18 December 2019 **Accepted:** 12 January 2020



Such properties are considered as essential industrial properties; which is why ZnO is being attracting researcher's attention. In this research, we used Braggs angles, Scherrer equation, Williamson-Hall and SSP analyses for ZnO nanoparticles (previously synthesised by our group using hydro-thermal technique at four different temperatures of 70, 100, 130 and 160 °C [6]) to study the temperature effect on ZnO crystallite lattice.

In terms of crystallography, a definite spatial arrangement of atoms in molecules is usually recognized as a unit cell. When unit cells periodically arrayed in a definite 3D lattice structure this could be recognized as a crystallite. When two crystallites, or even more, agglomerate together this would be recognized as a particle. In principles, perfect crystallites should never stop crystallising in all directions. Yet, infinite crystallinity is far beyond reality. As such, all known crystallites are imperfect crystallites i.e. crystallites with defects [7, 8]. Defects in crystallites affect surface morphology, oxidation state and charge transfer, which in turn, alter crystals optical, mechanical, electrical and chemical properties. Literatures classify crystallites defect as: zero-dimension defects e.g. interstitial and vacancies (also called point defects), one dimension defects e.g. dislocation (when atoms along a liner path become disordered), two dimensions defects e.g. when crystallites layers abnormally deviate from normal sequence, and finally, three dimensions defects e.g. holes, cracks or inclusions [9]. The size of smallest defect (i.e. point defects) may occur at an angstrom length scale; which is comparable with crystallites at a nanometre length scale, and hence, it cannot be negligible. In fact, sometimes defects induce extra properties for its materials which may considered as useful properties e.g. ZnO crystallites emit a blue emission of 467nm and green emission of 538nm as a result of zinc interstitial and oxygen vacancy defects [10].

Several theoretical methods are being applied for decades in order to estimate such defects and keep it under a controlled manner. Among these methods are Williamson-Hall and SSP methods. Williamson-Hall methods, also known as Williamson-Hall analyses (or W-H analyses for short), were first suggested in 1953 by G.K. Williamson and his student W.H.Hall. It was suggested to study the effect of crystallite size, strain, stress and energy density contributions on Braggs peak's position and Braggs peak's width

estimated via X-ray diffraction (XRD) spectroscopy [11].

In principles, in XRD spectroscopy, sharp and intense Braggs peaks indicate a well crystallinity. Crystallite size may contribute to affect the peak intensity and peak position. That is, larger crystallite size induces intense peaks and shift peaks positions towards smaller reflection angles and vice versa. This could be attributed to the large distances between crystallite planes, known as d , which was already expressed last century by Braggs law (explained below). Crystallite strain, stress and energy density may contribute to affect peaks width in a way that is large strain, high stress and anisotropic energy density would increase Braggs peaks' width; this is of course because they are considered as crystallites defects. Generally speaking, XRD data are considered as approximate measurements since they are based on integrated data, yet, they still provide reliable information regarding crystallites data base [7, 8].

Braggs law was first suggested in 1912 by Lawrence Bragg and his father William Bragg with the following expression [12, 13]:

$$n\lambda = 2d \sin\theta \quad 1$$

Where n is an integer number which refers to the order of diffraction and usually equals to unity, λ is the X-ray wavelength and θ is the diffraction angle (also known as Braggs angle). Braggs law proposes a relation between the internal lattice distances and the corresponding diffraction angles; which was, and yet till now, being successfully used for lattice constants estimations.

$$D = \frac{k\lambda}{\beta \cos\theta} \quad 2$$

In 1918 Paul Scherrer, a Swiss physicist, suggested another relation (which was then named after his name as Scherrer equation) to establish the relation between the crystallite size and the diffraction angle; which is also being successfully used but for the crystallites sizes estimations. Scherrer equation is shown in equation 2 below [14, 15]:

$$\cos\theta = \frac{k\lambda}{D} \left(\frac{1}{\beta}\right) \quad 3$$

Where K is the shape constant equals to 0.94, λ is the X-ray wavelength equals to 1.54056 Å, β is the peak width at half maximum, θ is the diffraction angle and D is the crystallite size. In fact, Scherrer equation could be re-arranged to have the expression given in equation 3. In this equation, if the X-axis of $((1)/(\beta))$ is plotted against the Y-axis of $\cos\theta$ it would be possible then to calculate the



crystallites size from the slope which equals to $(k\lambda)/(D)$.

In order to estimate size, strain, stress and energy density contributions on Bragg's peak's width, position, shape and intensity, Williamson-Hall method suggests three models known as Uniform Deformation Model or UDM for short, Uniform Deformation Stress Model or UDSM and Uniform Deformation Energy Density Model or UDEDM. A complement theoretical method is the Size-Strain Plot, or SSP for short; which could be used to estimate the relations between strain-stress and strain-energy density, and henceforth, to estimate their contributions on Bragg's peak's width, position, shape and intensity.

In principles, the expression given in equation 4 is used in UDM to estimate the contribution of lattice strain ϵ and the contribution of crystallite size to Bragg's peaks width. If the X-axis of $4 \sin^2\theta$ is plotted against the Y-axis of $\beta \cos\theta$, it would be possible then to calculate the lattice strain from the slope ϵ and the crystallite size from the intercept $((k\lambda)/D)$ [7, 8, 11].

$$\beta \cos\theta = \left(\frac{k\lambda}{D}\right) + (4\epsilon \sin\theta) \quad 4$$

The expression given in equation 5 is used in UDSM to estimate the contribution of lattice stress σ and the contribution of crystallite size to Bragg's peaks width. If the X-axis of $\left(\frac{4 \sin^2\theta}{Y}\right)$ is plotted against the Y-axis of $\beta \cos\theta$, it would be possible then to calculate the lattice stress from the slope σ and the crystallite size from the intercept $\left(\frac{k\lambda}{D}\right)$ [7, 8, 11].

$$\beta \cos\theta = \left(\frac{k\lambda}{D}\right) + \left(\frac{4 \sigma \sin\theta}{Y}\right) \quad (5)$$

Whereas Y is the Young's modulus equals to 130GPa for ZnO hexagonal crystallites.

The expression given in equation 6 is used in UDEDM to estimate the contribution of energy density U and the contribution of crystallite size to Bragg's peaks width. That is, if the X-axis $4 \sin\theta \left(\frac{2}{Y}\right)^{1/2}$ of is plotted against the Y-axis of $\beta \cos\theta$, it would be possible then to calculate the energy density from the slope \sqrt{U} and the crystallite size from the intercept $\left(\frac{k\lambda}{D}\right)$ [7, 8, 11].

$$\beta \cos\theta = \left(\frac{k\lambda}{D}\right) + \left(4 \sin\theta \left(\frac{2U}{Y}\right)^{1/2}\right) \quad (6)$$

Finally, the expression given in equation 7 is used in SSP method to establish the average relation between the lattice internal distances (evaluated by

d) and the lattice defects (concluded from β and $\cos\theta$) and the contribution of such relation on crystallite size D and crystallite strains ϵ . SSP method has the advantage of reducing the weight of the contributions coming from the lattice defects because it considers a comparable weight to the contributions coming from the lattice internal distances. This is why it could be considered as more realistic method than Scherrer and WH methods. In SSP method, if the X-axis of $(d\beta \cos\theta)^2$ is plotted against the Y-axis of $(d\beta \cos\theta)^2$, it would be possible then to calculate the crystallite size from the slope $(k)/D$ and the lattice strain from the intercept $(\epsilon/2)^2$ [7, 8, 11].

$$(d\beta \cos\theta)^2 = \frac{k}{D} (d^2 \beta \cos\theta) + \left(\frac{\epsilon}{2}\right)^2 \quad (7)$$

Experimental Work

Following the procedure of Ref [6], precursors of 0.5M zinc acetate dihydrate ($\text{Zn}(\text{CH}_3\text{COO})_2 \cdot 2\text{H}_2\text{O}$, BDH chemicals, 99% purity) and 5M sodium hydroxide (NaOH, Fluka, 97% purity), both were prepared using methanol (CH_3OH , GCC, 99% purity) as a solvent, were mixed under continuous magnetic stirring at a molar ratio of 1:10. The mixture was then put into a reactor of Teflon-lined-stainless steel autoclave and heated at fixed temperatures of 70, 100, 130 and 160 °C for 24 hours. All products were then filtered and washed with de-ionized water (laboratory utilities, $\sim 10\mu\text{s/cm}$) several times until the pH of final solution was 7.0. It was then had the final wash with ethanol (CH_3OH , GCC, 99% purity) before eventually been dried at 100 °C for 12h.

Samples were then characterized via XRD crystallography; this is an automated diffractometer from Bruker D8 Advance with Cu-K α radiation/ $\lambda=1.5406\text{nm}$, and SEM microscopy from FEI company /INSPECT S50 model.

Results and Discussions

XRD patterns for ZnO nanoparticles have indicated hexagonal crystallites unit cells which mostly assembled as crystallites with wurtzite like shapes. After problematics of instrumental broadening been sorted out, it has been found that all diffraction patterns for nine plane configurations of 100, 002, 101, 102, 110, 103, 200, 112 and 201 have perfectly matched the standard reference data of JCPDS: (36-1451) card for ZnO powder; which in turn, indicating the formation of pure ZnO crystallites at four different temperatures of 70,



100,130 and 160oC, see Figure1.

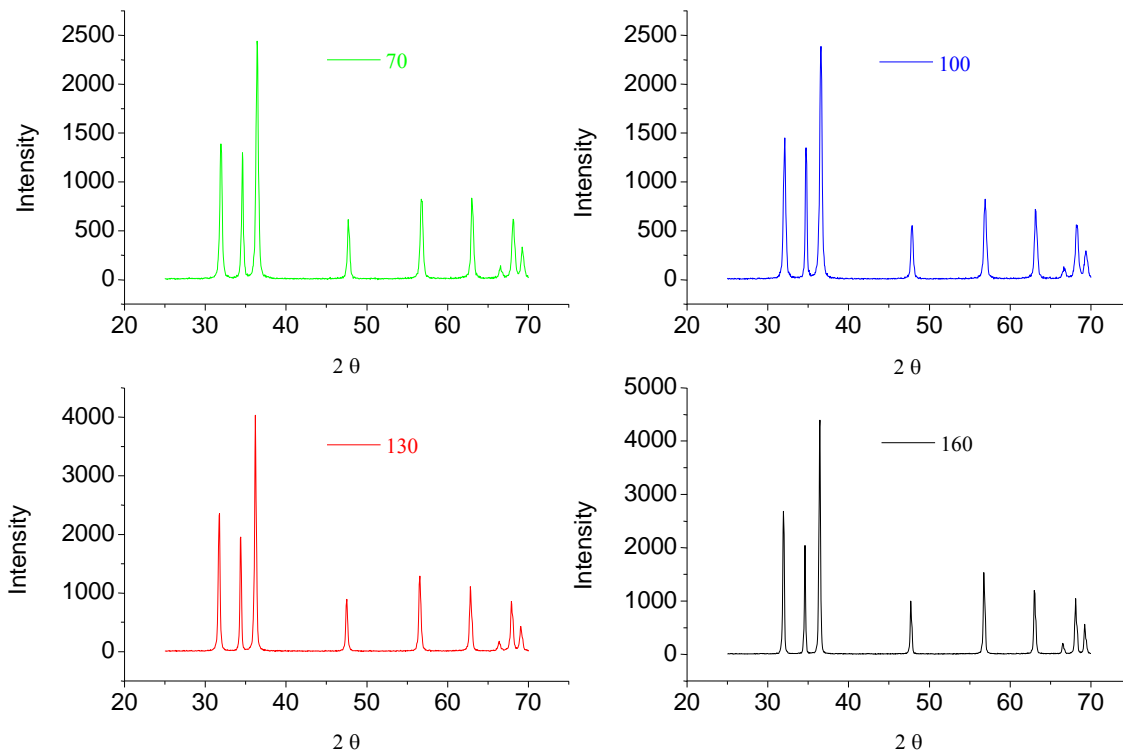


Figure 1: XRD patterns for ZnO nanostructures at four different temperatures of 70, 100, 130 and 160 oC. Reflection peaks corresponding to nine plane configurations namely as: 100, 002, 101, 102, 110, 103, 200, 112 and 201, which they have all perfectly matched with the standard reference data of JCPDS: (36-1451) card for ZnO powder; to indicate the hexagonal crystallites which mostly assembled as crystallites with wurtzite like shapes.

Following Braggs law, we estimated the crystallites internal distances *d* for the nine plane configurations mentioned above using equation 1. In Table 1 we presented our results and comparison results from Bindu et.al and results from JCPDS cards for six plane configurations of

100, 002, 101, 102, 110 and 103 [4]. With all different circumstances surrounding the different methodologies, i.e. different crystallizations environments, we have found that our results are in a good agreement with others results, which again, indicates the formation of pure ZnO crystallites.

Table 1: ZnO crystallites internal distances *d* calculated using Braggs Law for nine plane configuration of 100, 002, 101, 102, 110, 103, 200, 112 and 201 at four different temperatures of 70, 100, 130 and 160 oC; in addition to comparison with others results from reference [4] for six plane configurations of 100, 002, 101, 102, 110, 103.

Plane Configuration <i>hkl</i>	Lattice internal distance <i>d</i> _{XRD} in Angstrom Å					
	<i>d</i> _{XRD} (Ref [4])	<i>d</i> _{JCPDS} (Ref [4])	<i>d</i> _{XRD} (Results for this work)			
			70 °C	100 °C	130 °C	160 °C
100	2.7964	2.8135	2.52093	2.51029	2.53804	2.5204
002	2.5871	2.6027	2.33239	2.32334	2.34705	2.33245
101	2.4624	2.4751	2.21914	2.21087	2.23216	2.2189
102	1.903	1.9106	1.71432	1.71	1.72193	1.71455
110	1.6196	1.6244	1.45876	1.45563	1.46365	1.45871
103	1.4727	1.4769	1.3265	1.32407	1.33023	1.32656
112	0	0	1.26396	1.26163	1.26686	1.26397
200	0	0	1.23811	1.23609	1.24119	1.23816
201	0	0	1.22042	1.2184	1.22316	1.22033

In order to have a closer sight on crystallites unit cells, we have estimated the crystallites lattice constants *a* and *c* using the following equation [8]:

$$\frac{1}{d^2} = \frac{4}{3} \left(\frac{h^2 + hk + k^2}{a^2} \right) + \frac{l^2}{c^2}$$

Also, we estimated the unit cell volume *V* using the

following equation [8]:

$$V = \frac{\sqrt{3}a^2c}{2} \tag{9}$$

(8) In Table 2 we presented the lattice constants *a*, *b* and *c* in addition to lattice constants ratios *c/a* and



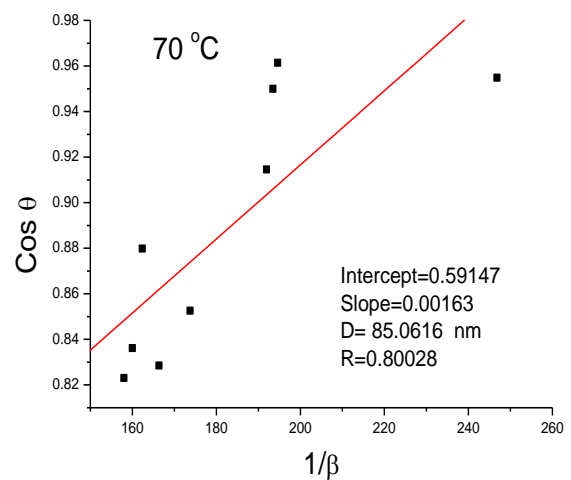
unit cells volume V for nine plane configurations of 100, 002, 101, 102, 110, 103, 200, 112 and 201 for ZnO crystallites prepared at four different temperatures of 70, 100, 130 and 160 oC. Fundamentally, lattice constants might give approximate idea about the spatial distribution of the atoms inside the molecule i.e. the geometry of the unit cell. For hexagonal shape, a and b represent the width and the length, respectively, of

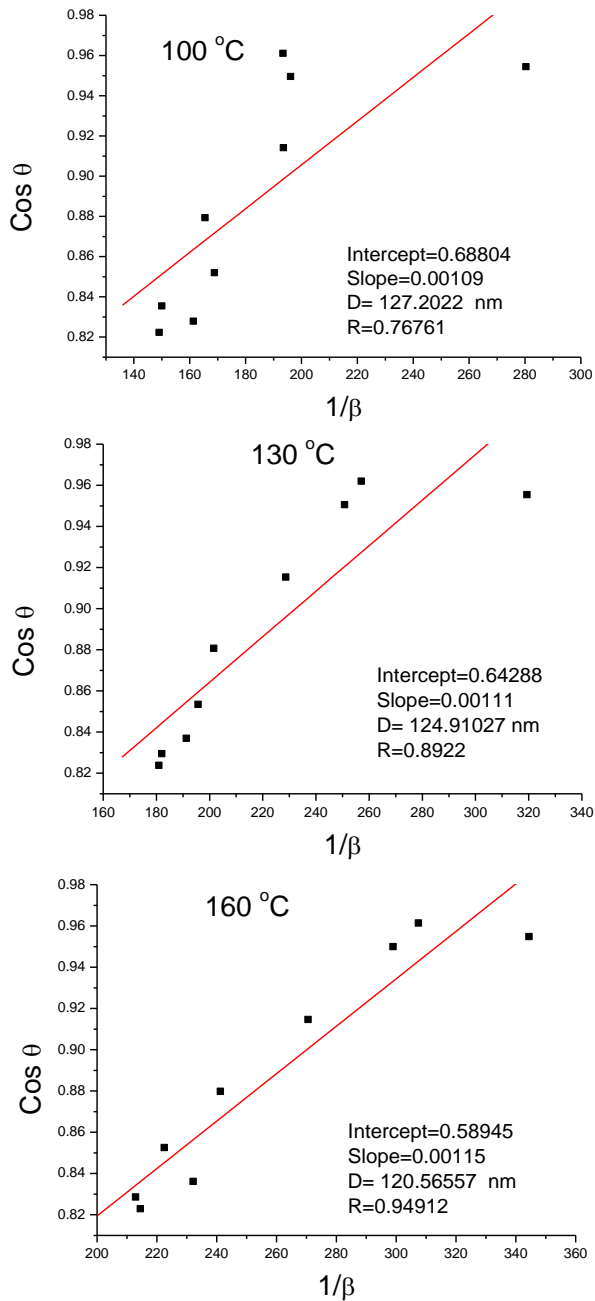
hexagonal face, and usually, a is supposed to be equal to b . While c represents the height of the hexagonal. As such, c/a may give an idea about the elongation of the hexagonal. In fact, c/a ratio should equal to 1.6, but, the case with our crystallites c/a ratio appeared to be equals to 1.4 at best; which obviously indicates the formation of hexagonal unit cells with short elongation.

Plane Configuration hkl	ZnO crystallites							
	Lattice constants in Angstrom Å							
	$a = b$				c			
	70 °C	100 °C	130 °C	160 °C	70 °C	100 °C	130 °C	160 °C
100	2.52093	2.51029	2.53804	2.5204	0	0	0	0
002	4.66477	4.64668	4.69411	4.6649	4.66477	4.64668	4.69411	4.6649
101	3.1383	3.12661	3.15673	3.13797	3.83415	3.81987	3.85667	3.83375
102	3.83321	3.82356	3.85023	3.83374	4.002	3.99193	4.01977	4.00256
110	2.06298	2.05856	2.0699	2.06291	0	0	0	0
103	4.19465	4.18697	4.20645	4.19483	4.27386	4.26603	4.28588	4.27404
112	3.09594	3.09023	3.10304	3.09598	4.36789	4.35983	4.37791	4.36795
200	2.47622	2.47217	2.48238	2.47632	0	0	0	0
201	2.72886	2.72435	2.73498	2.72865	--	--	--	--

Plane Configuration hkl	ZnO crystallites							
	Lattice constants ratio and unit cell volume							
	c/a				V (unit cell size) in Å			
	70 °C	100 °C	130 °C	160 °C	70 °C	100 °C	130 °C	160 °C
100	0	0	0	0	0	0	0	0
002	1	1	1	1	263.7199	260.6631	268.72722	263.74209
101	1.22173	1.22173	1.22173	1.22173	98.10942	97.01711	99.84763	98.0782
102	1.04403	1.04403	1.04403	1.04403	152.7758	151.6247	154.82	152.83915
110	0	0	0	0	0	0	0	0
103	1.01888	1.01888	1.01888	1.01888	195.373	194.3014	197.02604	195.39799
112	1.41085	1.41085	1.41085	1.41085	108.7696	108.1689	109.51965	108.77389
200	0	0	0	0	0	0	0	0
201	--	--	--	--	--	--	--	--

Figure 2 shows data distribution which we calculated using Scherre equation (equation 3) to estimate the crystallites sizes D for nine plane configurations of: 100, 002, 101, 102, 110, 103, 200, 112 and 201 at four different temperatures of: 70, 100, 130 and 160 oC. The average of data distribution was estimated via linear fitting algorithm which we calculated using Origin Lab software package. In fact, from a general look at this Figure one may note how the deviation from fitting lines tended to decrease as temperatures increase; which obviously indicate well crystallites improvement at high temperatures. In Table 3 we presented the average of crystallites sizes at each temperature, and we noticed how crystallites sizes have increased as temperatures increased.





average of data distribution was estimated via linear fitting algorithm which we calculated using OriginLab software package. Once again, one may note how the deviation from fitting lines tended to decrease as temperatures increase to indicate well crystallites improvement at high temperatures. In Table 3 we presented the average of crystallites sizes D and crystallites strains ϵ at each temperature and we noticed how crystallites sizes increased as temperatures increased, but, this is not the case with crystallites strains, especially at 160oC where defects started to decrease.

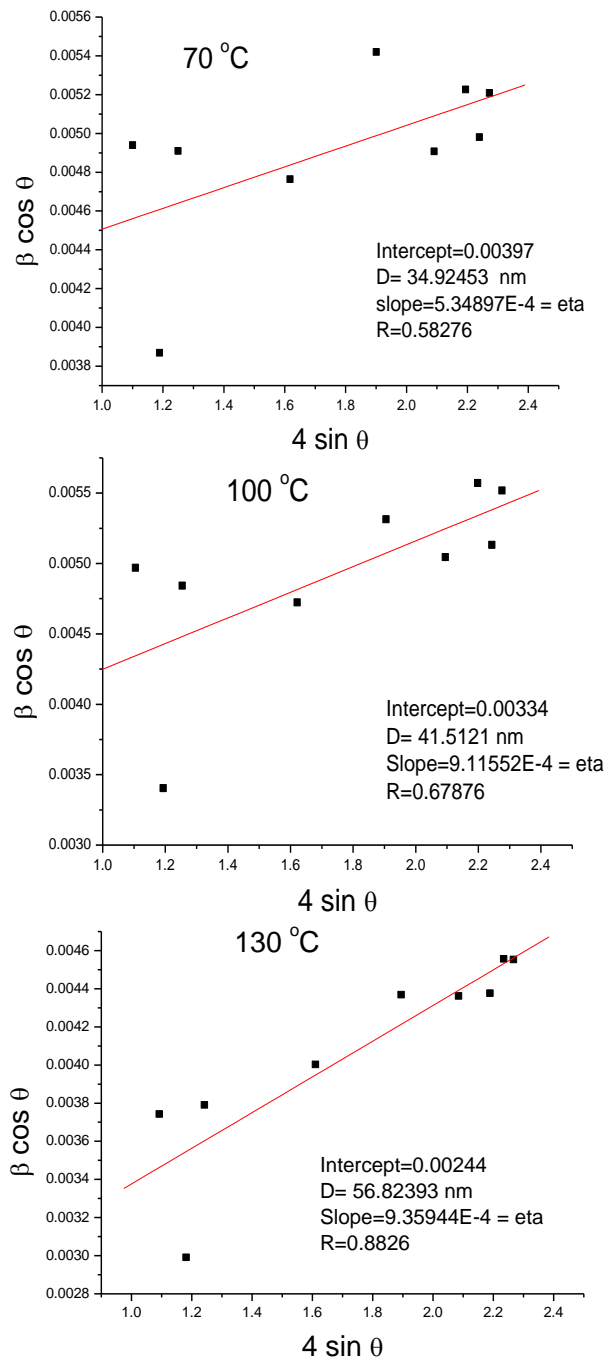


Figure 2: Scherrer based illustration for the relation between $\frac{1}{\beta}$ on X-axis and $\cos\theta$ on Y-axis to calculate the crystallites size from the slope which equals to D .

Chi squares values, represented by R, are shown to indicate how data deviations from fitting lines were gradually decreased as temperatures increased; which indicates well crystallinity improvements at high temperatures. Plane configuration of 002 has been emphasized with red colour next to its corresponding datum to show how its deviation was big from fitting lines in comparison to other configurations.

Figure 3 shows data distribution which we calculated using UDM (equation 4) to estimate the crystallites size D and crystallites strains ϵ for nine plane configurations of: 100, 002, 101, 102, 110, 103, 200, 112 and 201 at four different temperatures of: 70, 100, 130 and 160 oC. The



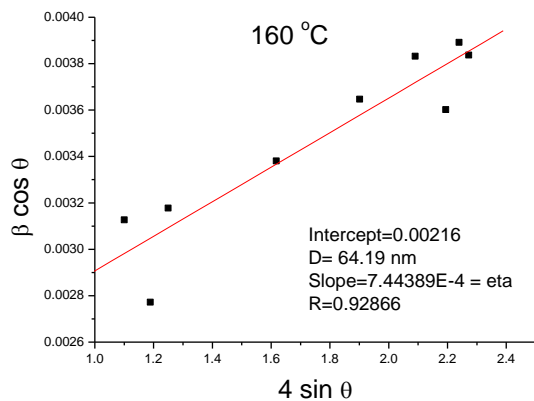


Figure 3: UDM based illustration for the relation between $4 \sin \theta$ on X-axis and $\beta \cos \theta$ on Y-axis to calculate the lattice strain from the slope which equals to ϵ and the crystallite size from the intercept

which equals to $\left(\frac{k\lambda}{D}\right)$. Chi squares values, represented by R, are shown to indicate how data deviations from fitting lines were gradually decreased as temperatures increased; which indicates well crystallinity improvements at high temperatures. Plane configuration of 002 has been emphasized with red colour next to its corresponding datum to show how its deviation was big from fitting lines in comparison to other configurations.

Figure 4 shows data distribution which we calculated using UDSM (equation 5) to estimate the crystallites size D, crystallites stress σ and crystallites strains ϵ for nine plane configurations of: 100, 002, 101, 102, 110, 103, 200, 112 and 201 at four different temperatures of: 70, 100, 130 and 160 oC. The average of data distribution was estimated via linear fitting algorithm which we calculated using OriginLab software package. Again, one may note how the deviation from fitting lines tended to decrease as temperatures increase; to indicate well crystallites improvement at high temperatures. In Table 3 we presented the average of crystallites sizes D, crystallites stress σ and crystallites strains ϵ at each temperature and we noticed how crystallites sizes increased as temperatures increased, again, this is not the case with crystallites stress and crystallites strains, especially at 160oC where defects started to decrease.

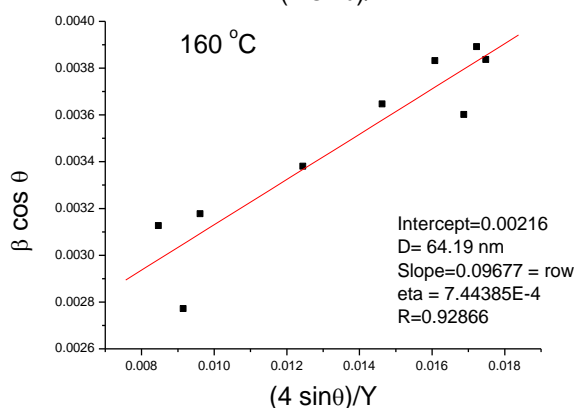
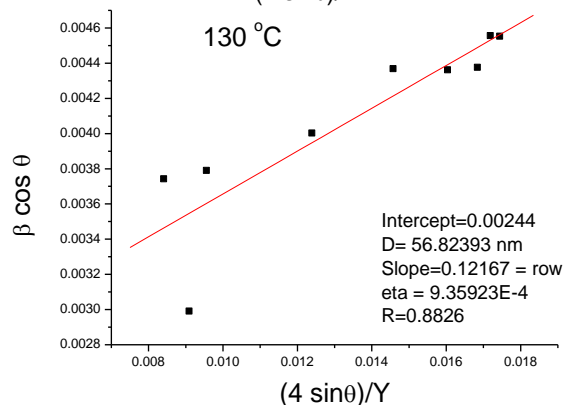
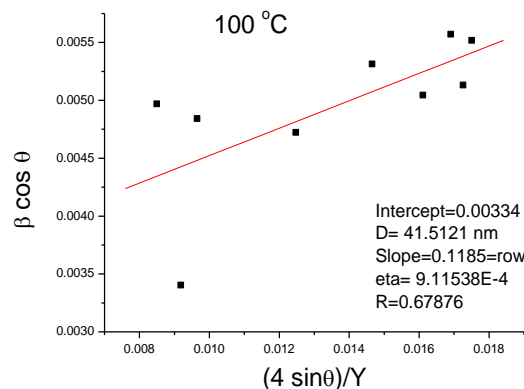
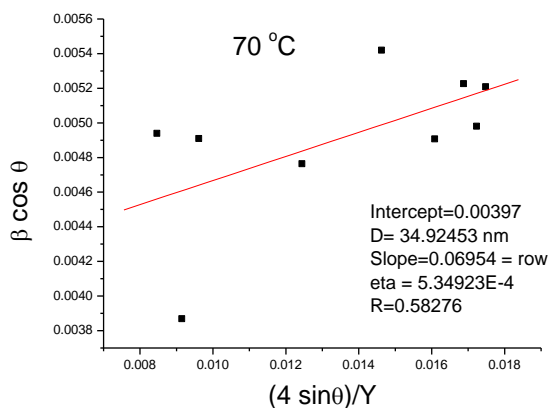


Figure 4: UDSM based illustration for the relation between $\left(\frac{4 \sin \theta}{Y}\right)$ on X-axis and $\beta \cos \theta$ on Y-axis to calculate the lattice stress from the slope which equals to σ and the crystallite size from the intercept

which equals to $\left(\frac{k\lambda}{D}\right)$. Chi square values, represented by R, are shown to indicate how data deviations from fitting lines were gradually decreased as temperatures increased; which indicates well crystallinity improvements at high temperatures. Plane configuration of 002 has been emphasized with red colour next to its corresponding datum to show how its deviation was big from fitting lines in comparison to other configurations.

Figure 5 shows data distribution which we calculated using UDEDM (equation 6) to estimate the crystallites size D and crystallites energy density u for nine plane configurations of: 100, 002, 101, 102, 110, 103, 200, 112 and 201 at four different temperatures of: 70, 100, 130 and 160 oC. The Average of data distribution was estimated via linear fitting algorithm which we calculated using



OriginLab software package. Yet again, one may note how the deviation from fitting lines tended to decrease as temperatures increase; indicating well crystallites improvement at high temperatures. In Table 3 we presented the average of crystallites sizes D and crystallites energy density u at each temperature and we noticed how crystallites sizes increased as temperatures increased, but then again, this is not the case with crystallites energy density u, especially at 160oC where defects started to decrease.

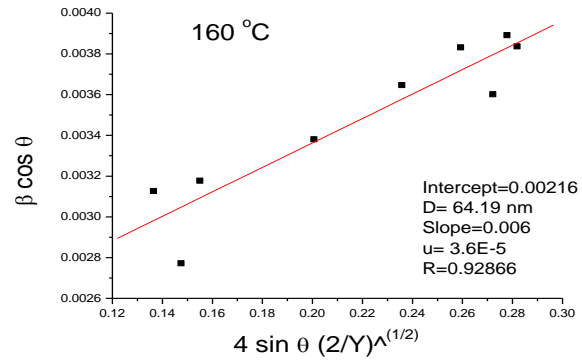
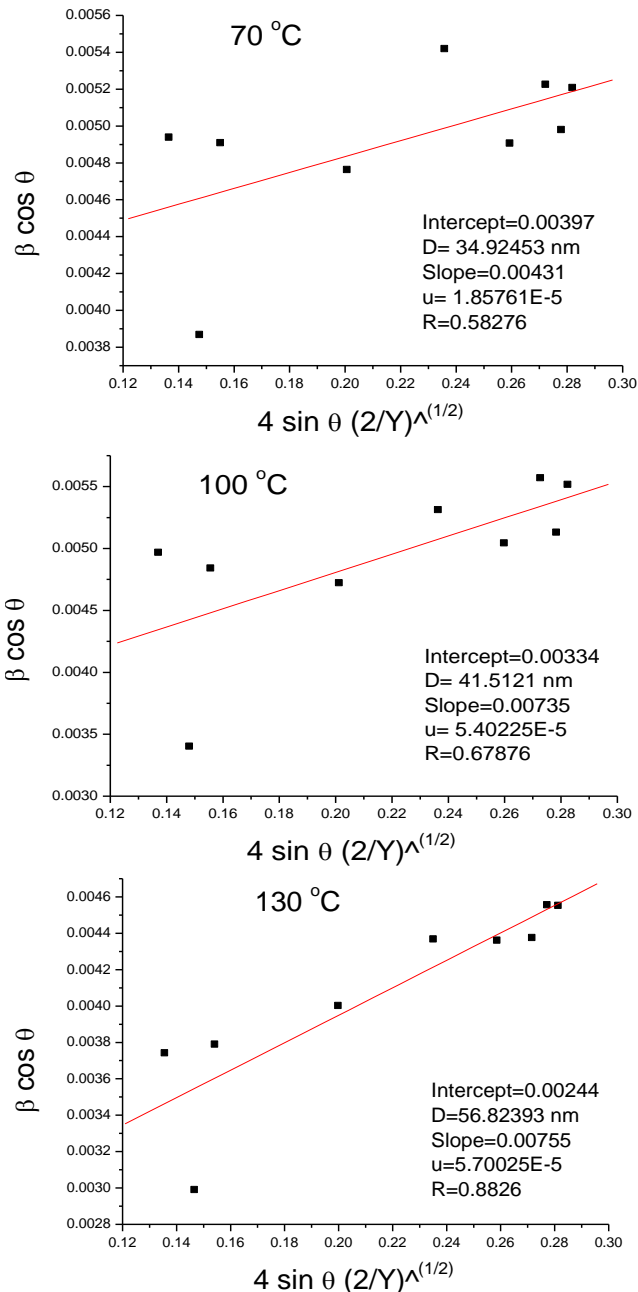
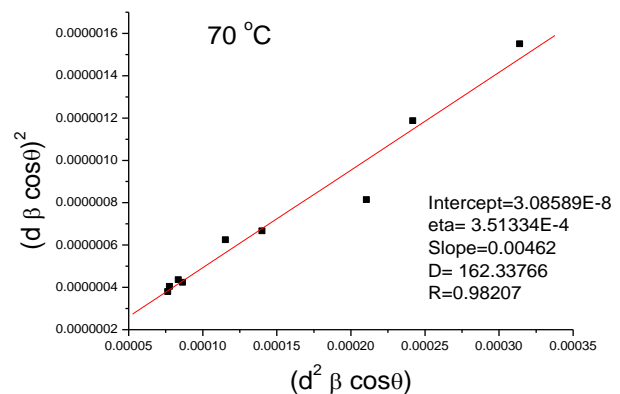


Figure 5: UDEDM based illustration for the relation between $4 \sin \theta \left(\frac{2}{\gamma}\right)^{1/2}$ on X-axis and $\beta \cos \theta$ on Y-axis to calculate the energy density from the slope which equals to \sqrt{u} and the crystallite size from the intercept which equals to $\left(\frac{k\lambda}{D}\right)$. Chi squares values, represented by R, are shown to indicate how data deviations from fitting lines were gradually decreased as temperatures increased; which indicates well crystallinity improvements at high temperatures. Plane configuration of 002 has been emphasized with red colour next to its corresponding datum to show how its deviation was big from fitting lines in comparison to other configurations.

Figure 6 shows data distribution which we calculated using SSP (equation 7) to estimate the crystallites size D and crystallites strains ϵ for nine plane configurations of: 100, 002, 101, 102, 110, 103, 200, 112 and 201 at four different temperatures of: 70, 100, 130 and 160 oC. The average of data distribution was estimated via linear fitting algorithm which we calculated using OriginLab software package. Similar to WH findings, we noticed that the deviation from fitting lines tended to decrease as temperatures increase which may indicate well crystallites improvement at high temperatures. In Table 3 we presented the average of crystallites sizes D and crystallites strains ϵ at each temperature and we noticed how crystallites sizes increased as temperatures increased, but again, this is not the case with crystallites strains, especially at 160oC where defects started to decrease.



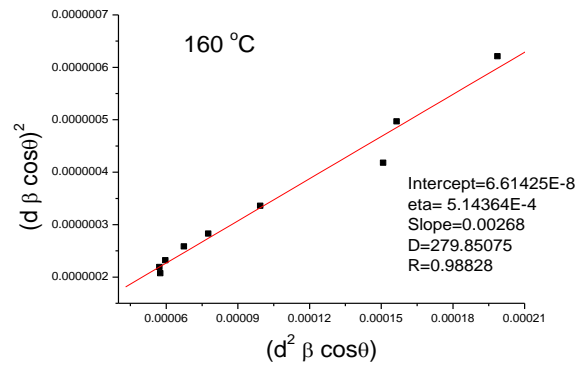
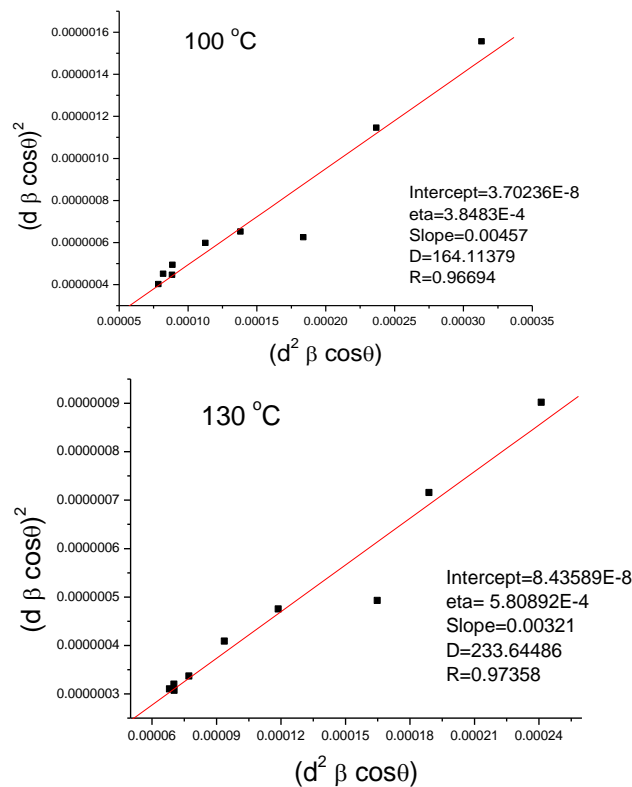


Figure 6: SSP based illustration for the relation between $(d^2 \beta \cos\theta)^2$ on X-axis and $(d \beta \cos\theta)^2$ on Y-axis to calculate the crystallites size from the slope which equals to $\frac{k}{D}$ and the lattice strain from the intercept which equals to $\left(\frac{\epsilon}{2}\right)^2$. Chi square values, represented by R, are shown to indicate how data deviations from fitting lines were gradually decreased as temperatures increased; which indicates well crystallinity improvements at high temperatures. Plane configuration of 002 has been emphasized with red colour next to its corresponding datum to show how its deviation was big from fitting lines in comparison to other configurations.

Table 3: Averages of crystallites sizes, strain, stress and energy density for ZnO nanoparticles calculated using Scherrer equation, WH and SSP methods for nine plane configurations of: 100, 002, 101, 102, 110, 103, 200, 112 and 201 at four different temperatures of: 70, 100, 130 and 160 °C. The average crystallites size from all these methods was 40.39358nm.

T °C	Scherrer	SSP	
	D (nm)	D (nm)	ε (no unit)
70	28.45187	16.23377	3.51E-04
100	28.5799	16.41138	3.85E-04
130	34.5207	23.36449	5.81E-04
160	40.38552	27.98507	5.14E-04

T °C	UDM		UDSM			UEDM	
	D (nm)	ε (no unit)	D (nm)	σ (MPa)	ε (no unit)	D (nm)	U (kJ·m ⁻³)
70	34.924	5.35E-04	34.85446	0.06954	5.35E-04	34.92452	1.86E-05
100	41.51118	9.12E-04	41.39268	0.1185	9.12E-04	41.51204	5.40E-05
130	56.823	9.36E-04	56.70133	0.12167	9.36E-04	56.82388	5.70E-05
160	64.18926	7.44E-04	64.09249	0.09677	7.44E-04	64.18996	3.60E-05

Generally speaking, in Figures (2-6) we noticed that the diffraction of 002 plane configuration has spaced itself away from the fitting line of the average values in comparison to other configurations. This could be attributed to crystallite defect in this particular plane which led to enlarge the overall crystallites size since crystallites sizes are considered as a reflection of scattering diffraction domains. This defect might also be the reason why c/a ration has appeared to be much smaller than usual; especially, 002 planes configurations represent the face plane for ZnO hexagonal unit cell [16], and hence, when the face turns out to be large in comparison to the height; the final shape will end up then with short

elongation shape, see Figure (7-in set). Yet, in case with SSP method, this effect was not that big; because in SSP, less weight is given to Braggs diffraction angle (θ) in comparison to weights given to internal spaces d and peak broadening β. Also, for 002 plane configurations, we noticed that the tendency of spacing away from the fitting line of the average values tended to decrease as temperatures increase. In fact, we believe that this might happened because when temperatures increase the crystallites sizes would increase accordingly, and hence, the effects of small defects of a single plane (out of nine other planes) would no longer be appreciable.

Worthy note, in Table 3, crystallites sizes estimated



via Scherrer equation appeared to be much smaller than crystallites sizes estimated via WH methods. This should be expected because in Scherrer equation; crystallites strains, stress and energy density have no contributions on peaks width. Nonetheless, crystallites sizes estimated via SSP method appeared to be the smallest ever. As it is already mentioned above, this is because SSP method does not only reduce the contribution coming from crystallites defects, but it also considers a comparable weight coming from the contribution of lattice internal distances d . It is our point of view though; SSP is more realistic since it gives the smallest crystallite sizes ever.

Finally, we estimated the average number of unit cells inside the single crystallite, which we referred to as A . This was by dividing the average of crystallite sizes estimated via Scherrer equation (D Scherrer) by the average of crystallite unit cells volumes estimated in table 2b (V_{average}). This could be expressed as $A = D_{\text{Scherrer}} / V_{\text{average}}$. We noticed that A exponentially increased as temperatures increased from 70 to 160 oC, see Figure 7. This attitude is expected and it could be attributed to a natural phenomenon called Ostwald ripening; in which small crystallites immigrate to deposit and then to diffuse itself on bigger crystallites. It is believed that this might happen because of high kinetic energy potentialized inside the small crystallites where surface to volume ratio (S/V) is really high [17, 18]. Ostwald ripening phenomenon may also illustrates the gradual nanoparticles growth for the same reason. In Figure 8, SEM images have shown a gradual nanoparticles growth starting from particles with an average length of (30-100) nm to end up with elongated wurtzite like shapes (agglomerate as rod like shapes) particles with an average width less than 50nm and an average length less than 500nm.

Conclusion

Estimation via Braggs law, Scherrer equation, WH and SSP methods have all shown a comparable results with each other as well as with others results; despite the fact that estimations were based on different views of prospective. Crystallinity was highly improved as temperatures increased; this could be realized from data distribution around the average fitting lines i.e. from chi square values. All methods have indicated the existence of pure ZnO crystallites with a short elongation hexagonal; which agglomerated as

nanoparticles with an average size of 40 nm crystallites with wurtzite like shapes. SEM images have indicated a gradual nanoparticles growth when temperatures increased from 70 oC to 160 oC.

Acknowledgment

We would like to thank Assistant Professor Dr. Abdulkareem A Alsammarraie for scientific and instrumental consultants, also, would like to thank the University of Baghdad and Department of Chemistry/College of Science for facilitating the opportunity to conduct this work.

References

- Battez AH, Gonzalez R, Viesca J, Fernandez J, Diazfernandez J, MacHado A, Chou R, Riba J. "CuO, ZrO and ZnO nanoparticles as antiwear additive in oil lubricants", *Wear*, 2008; 265(3-4): (422-428).
- ZnO database by Royal Society of Chemistry, www.chemspider.com/chemical-structure.14122.html. Cited on Aug. 2019.
- Yoshikawa A. "Development of Applications of Wide Bandgap Semiconductors", *Wide Bandgap Semiconductors*, Springer, 2007; 1-24. ISBN978-3-540-47235-3.
- Bindu P, Thomas S. "Estimation of lattice strain in ZnO nanoparticles: X-ray peak profile analysis", *Journal of Theoretical and Applied Physics*, 2014; 8: 123–134.
- Madelung O, Schulz M, Weiss H. *Landolt-Boörnstein New Series*. Springer, Berlin, 1982.
- Abdulrahman A, Mohammed H. "Temperature and Solvent Impact on Zinc Oxide Nanostructures Synthesized via Hydro-Solvo-Thermal Technique", *International Journal of Science and Research (IJSR)*, 2017; 6(11): 1132-1136.
- Mote V, Purushotham Y, Dole B. "Williamson-Hall analysis in estimation of lattice strain in nanometer-sized ZnO particles", *Journal of Theoretical and Applied Physics*, 2012; 6(6): 1-8.
- Khorsand A, Majid W, Abrishami M, Yousefi R. "X-ray analysis of ZnO nanoparticles by Williamson- Hall and size-strain plot methods", *Solid State Science*, 2011; 13: 251-256.
- Fang TT. "Elements of Structures and Defects of Crystalline Materials/ Part II. Defects of Crystalline Materials", Elsevier Science, 2018; 81.
- Kalita A, Kalita M. "Williamson-Hall analysis and optical properties of small sized ZnO nanocrystals", *Physica E*, 2017; 92: 36-40.
- Williamson G. Hall W., "X-ray line broadening from field aluminium and wolfram", *Acta Metall*, 1953; 1: 22-31.
- Bragg W, Bragg L. "The Reflexion of X-rays by Crystals", *Proceedings of the Royal Society of London, Series A*, 1913; 88(605): 428-438.
- Myers H. "Introductory Solid State Physics", Taylor & Francis e-Library, 2009; 2nd Edition: 55.
- Scherrer P. *Göttinger Nachrichten Gesell*, 1918; 2: 98.



Patterson A. "The Scherrer Formula and X-Ray Particle Determination", Physical Review Journals Archive/APS, 1939; 56(10): 978-982.

Hu Y, Chen Y, Xu H, Gao H, Jaing W, Hu F, Wang Y. "Texture ZnO Thin-Films and their Application as Front Electrode in Solar Cells", Engineering, 2010; 2(10): 973-978.

Ostwald W. Lehrbuch der Allgemeinen, Chemie/Leipzig, Germany, 1896; 2(1).

Ostwald W."Studin über die Bildung und, Umwandlung fester Körper" (Studies on the Formation and Transformation of Solid Bodies), Zeitschrift für Physikalische Chemie, 1897; 22: 289-322.